

## Entrainment in bottom gravity currents over complex topography from three-dimensional nonhydrostatic simulations

Tamay M. Özgökmen,<sup>1</sup> Paul F. Fischer,<sup>2</sup> Jinqiao Duan,<sup>3</sup> and Traian Iliescu<sup>4</sup>

Received 6 April 2004; accepted 11 June 2004; published 10 July 2004.

[1] By recognizing that oceanic overflows follow the seafloor morphology, which shows a self-similar structure at spatial scales ranging from 100 km to 1 m, the impact of topographic bumps on entrainment in gravity currents is investigated using a 3D nonhydrostatic spectral element model. It is found that a bumpy surface can lead to a significant enhancement of entrainment compared to a smooth surface. The change in entrainment is parameterized as a function of statistical estimates of the amplitude and wavenumber parameters of bumps with respect to the background slope. **INDEX TERMS:** 4255 Oceanography: General: Numerical modeling; 4243 Oceanography: General: Marginal and semienclosed seas; 4524 Oceanography: Physical: Fine structure and microstructure; 4568 Oceanography: Physical: Turbulence, diffusion, and mixing processes; 4512 Oceanography: Physical: Currents. **Citation:** Özgökmen, T. M., P. F. Fischer, J. Duan, and T. Iliescu (2004), Entrainment in bottom gravity currents over complex topography from three-dimensional nonhydrostatic simulations, *Geophys. Res. Lett.*, 31, L13212, doi:10.1029/2004GL020186.

### 1. Introduction

[2] Most deep and intermediate water masses are released into the large-scale ocean circulation from high-latitude and marginal seas in the form of overflows. The seminal work by Price *et al.* [1993] and Price and Baringer [1994] revealed that the mixing of overflows with the ambient fluid takes place over very small spatial and time scales. Studies with ocean general circulation models demonstrated that the strength of the thermohaline circulation is very sensitive to details of the representation of overflows in these models [e.g., Willebrand *et al.*, 2001]. In light of these results, overflow-induced entrainment is being generally recognized as one of the prominent oceanic processes, with a direct impact on climate research. The importance of overflows has led to significant effort to improve their representation in ocean models, and much progress has been achieved recently [e.g., Beckmann and Dörscher, 1997; Papadakis *et al.*, 2003]. Despite the recent progress, a number of outstanding and difficult problems need to be

addressed given that the ultimate objective is to parameterize the mixing of overflows taking place over scales of  $O(100\text{ m})$  and  $O(\text{few hours})$  for climate models with 100 km resolution that need to be integrated for  $O(100\text{ years})$  (W. Large and R. Hallberg, personal communication). One of the issues that deserves attention is the potential impact of seafloor topography on entrainment in overflows. Unlike smooth surfaces used in laboratory experiments [see Baines, 2001, and references therein], the seafloor surface shows a complex structure. While a deterministic representation is possible for horizontal scales larger than 10–100 km, a self-similar (fractal) behavior applies for scales of 100 km–1 m. Power laws [Weissel *et al.*, 1994] and stochastic models [Goff and Jordan, 1988] relating horizontal scale to height have been successfully developed in the geological community. Relatively small attention has been paid to the interaction of overflows with seafloor morphology [Özsoy *et al.*, 2001], possibly because of lack of high-resolution overflow data sets, and suitable nonhydrostatic models.

[3] Our objective in this study is to explore and quantify the impact of small-scale [ $O(1\text{ km})$ ] bumps on the entrainment in bottom gravity currents via a systematic set of numerical experiments using a high-resolution, 3D nonhydrostatic spectral element model. Our hypothesis is that, given the overflows follow bottom topography until they form deep water masses, the properties of the product water should be sensitive to the details of topography, which, by inducing acceleration and deceleration due to changes in the slope angle, can excite internal waves and changes in the shear production that can ultimately affect entrainment.

### 2. Method

[4] A high-order parallel spectral element Navier Stokes solver, Nek5000, is used as the basis of the numerical simulations. This model, which is documented in detail by Fischer [1997] and Fischer and Mullen [2001], integrates the Boussinesq equations for momentum,  $\frac{D\mathbf{u}}{Dt} = -\nabla p + \nabla_r^2 \mathbf{u} - Ra \hat{S}\hat{z}$ , conservation of mass,  $\nabla \cdot \mathbf{u} = 0$ , and salinity  $\frac{DS}{Dt} = Pr^{-1} \nabla_r^2 S$ , where the total derivative is  $\frac{D}{Dt} := \frac{\partial}{\partial t} + \mathbf{u} \cdot \nabla$ , and the anisotropic diffusivity is  $\nabla_r^2 := \frac{\partial^2}{\partial x^2} + \frac{\partial^2}{\partial y^2} + r \frac{\partial^2}{\partial z^2}$ . The variables are the velocity vector field  $\mathbf{u} = (u, v, w)$  and the pressure  $p$ , and the nondimensional parameters are  $Ra = (g \beta \Delta S H^3) / \nu_h^2$  the Rayleigh number, the ratio of the strengths of buoyancy and viscous forces, where  $g = 9.81\text{ m}^2\text{ s}^{-1}$ ,  $H$  is the domain depth and  $\Delta S$  is the salinity range,  $\beta = 7 \times 10^{-4}\text{ psu}^{-1}$  is the salinity contraction coefficient;  $Pr = \nu_h / K_h$  the Prandtl number, the ratio of viscous and saline diffusion; and  $r = \nu_v / \nu_h = K_v / K_h$ , the ratio of vertical and horizontal diffusivities.

[5] Our approach is to explore and quantify results from a reference experiment of gravity current flow over a smooth, constant-slope topography in comparison to those in which

<sup>1</sup>Rosenstiel School of Marine and Atmospheric Sciences/Meteorology and Physical Oceanography (RSMAS/MPO), University of Miami, Miami, Florida, USA.

<sup>2</sup>Mathematics and Computer Science Division, Argonne National Laboratory, Argonne, Illinois, USA.

<sup>3</sup>Department of Applied Mathematics, Illinois Institute of Technology, Chicago, Illinois, USA.

<sup>4</sup>Department of Mathematics, Virginia Polytechnic Institute and State University, Blacksburg, Virginia, USA.

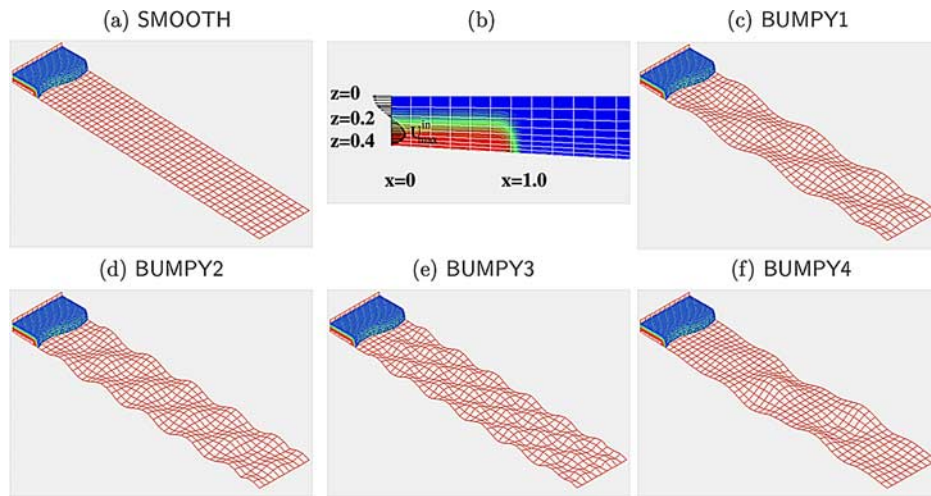


**Figure 1.** Bottom topography (shown for the cases of maximum amplitude parameters  $\eta$ ) in experiments (a) SMOOTH ( $\eta = 0$ ), (c) BUMPY1 ( $\eta = 0.40$ ), (d) BUMPY2 ( $\eta = 0.36$ ), (e) BUMPY3 ( $\eta = 0.30$ ) and (f) BUMPY4 ( $\eta = 0.31$ ). (b) Velocity profile at the inlet boundary superimposed on the initial distribution of salinity. Distribution of elements is depicted in the background.

bumps of various shapes and amplitudes are superimposed on the background topography.

[6] The basic experimental setup closely follows those by Özgökmen and Chassignet [2002] and Özgökmen *et al.* [2004], in which 2D and 3D bottom gravity current simulations were compared to results from laboratory experiments. The model domain has a horizontal length of  $L_x = 10$  km and a spanwise width of  $L_y = 2$  km. The depth of the water column ranges from 400 m at  $x = 0$  to  $H = 1000$  m at  $x = 10$  km, hence the background slope angle is  $\theta = 3.5^\circ$  (Figure 1a). The model is driven by the velocity and salinity forcing profiles at the inlet boundary at  $x = 0$  (Figure 1b). The initial thickness of the dense water mass is  $h_0 = 200$  m. The model parameters are  $Ra = 5 \times 10^6$ ,  $Pr = 1$  and  $r = 0.05$ . The reader is referred to Özgökmen *et al.* [2004] for a detailed discussion of model setup and selection of parameters.

[7] The reference experiment, denoted SMOOTH is accompanied by BUMPY experiments, in which the bottom topography is modified using  $z_{BUMPY}^b(x, y) = z_{SMOOTH}^b(x, y) +$

$\sum_{i=1}^6 A_i \sin\left(2\pi \frac{(x-x_0)}{\lambda_i^x}\right) \cos\left(2\pi \frac{y}{\lambda_i^y}\right)$ , where  $z_{BUMPY}^b$  and  $z_{SMOOTH}^b$  are the bottom levels,  $A_i$  is the amplitude, and  $\lambda_i^x$  and  $\lambda_i^y$  refer to the horizontal wavelengths of the bumps. The perturbations are started for  $x \geq x_0 = 1.5$  km to clear the initial volumes of the dense water (Figure 1).

[8] The topographic perturbations are characterized by defining an amplitude factor  $\eta \equiv \langle (z_{BUMPY}^b(x, y) - z_{SMOOTH}^b(x, y))^2 \rangle^{1/2} / h_0$ , where  $\langle \rangle$  denotes spatial  $(x, y)$  averaging over the domain, and a wavenumber factor

$$\kappa \equiv h_0 2\pi \sqrt{\left(\frac{\sum_i |A_i| \lambda_i^x}{\sum_i |A_i|}\right)^{-2} + (\lambda^y)^{-2}}.$$

Experiments are conducted using 4 different shapes ( $\kappa$ ) of topography, denoted BUMPY1 (regular low wavenumber), BUMPY2 (regular medium wavenumber), BUMPY3 (regular high wavenumber), and BUMPY4 (irregular low wavenumber) (Figures 1c–1f). Experiments of 4 or 5 different amplitudes ( $\eta$ ) are then conducted for each type of topography. The amplitude is chosen to be  $\eta \leq 0.4$  such that topographic blocking is not significant. A total of 18 BUMPY experi-

**Table 1.** Parameters of bottom topography in the 18 BUMPY experiments

Topography	$\lambda_i^x, \lambda_i^y$ (km)	$\kappa$	$A_i$ (m)	$\eta$
BUMPY1	$\lambda_3^x = 2.83$ $\lambda^y = 2$	0.77	$A_1 = A_2 = A_4 = A_5 = A_6 = 0$ (1) $A_3 = 24$ ; (2) $A_3 = 58$ (3) $A_3 = 82$ ; (4) $A_3 = 116$ (5) $A_3 = 165$	(1) 0.06; (2) 0.15 (3) 0.21; (4) 0.29 (5) 0.40
BUMPY2	$\lambda_5^x = 1.70$ $\lambda^y = 2$	0.97	$A_1 = A_2 = A_3 = A_4 = A_6 = 0$ (6) $A_5 = 33$ ; (7) $A_5 = 47$ (8) $A_5 = 66$ ; (9) $A_5 = 94$ (10) $A_5 = 144$	(6) 0.08; (7) 0.12 (8) 0.17; (9) 0.23 (10) 0.36
BUMPY3	$\lambda_3^x = 1.42$ $\lambda^y = 1$	1.54	$A_1 = A_2 = A_3 = A_4 = A_5 = 0$ (11) $A_6 = 40$ ; (12) $A_6 = 60$ (13) $A_6 = 84$ ; (14) $A_6 = 120$	(11) 0.10; (12) 0.15 (13) 0.22; (14) 0.30
BUMPY4	$\lambda_1^x = 8.5$ $\lambda_2^x = 4.3$ $\lambda_3^x = 2.8$ $\lambda_4^x = 2.1$ $\lambda_5^x = 1.7$ $\lambda^y = 2$	0.68	$A_6 = 0$ (15) $A_1 = -28, A_2 = 20, A_3 = -16,$ $A_4 = -14, A_5 = 13$ (16) $A_1 = -40, A_2 = 28, A_3 = -23,$ $A_4 = -20, A_5 = 17$ (17) $A_1 = -56, A_2 = 42, A_3 = -32,$ $A_4 = -28, A_5 = 25$ (18) $A_1 = -79, A_2 = 56, A_3 = -46,$ $A_4 = -40, A_5 = 35$	(15) 0.11 (16) 0.16 (17) 0.22 (18) 0.31

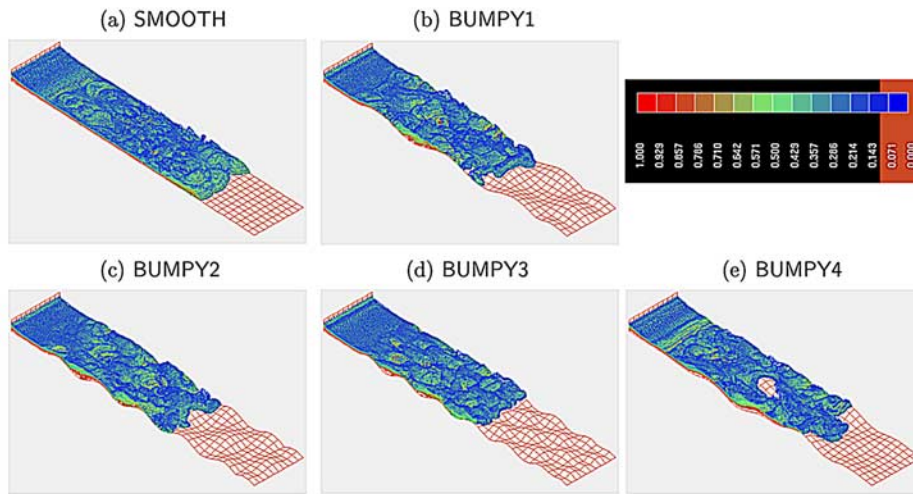


**Figure 2.** Distribution of salinity at  $t = 7863$  s in selected experiments (a) SMOOTH ( $\eta = 0$ ), (b) BUMPY1 ( $\eta = 0.40$ ), (c) BUMPY2 ( $\eta = 0.36$ ), (d) BUMPY3 ( $\eta = 0.30$ ) and (e) BUMPY4 ( $\eta = 0.31$ ). A sample animation is available from: <http://www.rsmas.miami.edu/personal/tamay/3D/BUMPY4.gif>.

ments are conducted, the parameters of which are shown in Table 1.

### 3. Results

#### 3.1. Description

[9] The evolutions of salinity distribution in SMOOTH and selected BUMPY are shown in Figure 2. The initial development of the system is that of the so-called lock-exchange flow, in which the lighter fluid remains on top and the denser overflow propagates downslope. In the case of SMOOTH (Figure 2a), the dense gravity current quickly develops a characteristic “head” at the leading edge of the current, and spanwise Kelvin-Helmholtz rolls in the trailing fluid, which are well-known features from laboratory experiments. Kelvin-Helmholtz rolls gradually transition to 3D via secondary instabilities. The flow along the leading edge of the current is composed of a complex pattern of so-called lobes and clefts that are highly unsteady features formed by the instability of the leading edge. As exhibited in Figures 2b–2e, the flow can be strongly affected by the presence of topographic features; most notably, a characteristic head cannot be clearly identified anymore (the head can account for a large portion of the total entrainment [e.g., Turner, 1986]) and the overturning structures seem qualitatively different in all BUMPY experiments. Therefore, one would anticipate changes in how much ambient fluid is entrained into the gravity current.

#### 3.2. Entrainment

[10] Turner [1986] defined an entrainment parameter in bottom gravity currents as the change of the dense flow thickness  $h$  along the streamwise direction  $X$ ,  $E \equiv dh/dX$ , a 2D expression, which can be mapped to 3D flows as [Özgökmen *et al.*, 2004]  $E(t) \equiv (\bar{h}(t) - \bar{h}_0(t))/\bar{\ell}(t)$ , where  $\bar{\ell}(t) = \langle X_F(y, t) - x_0 \rangle_y$  is the spanwise-averaged length of the dense overflow measured between the reference station  $x_0$  and the leading edge  $X_F(y, t)$ ,  $\bar{h}(t)$  is the total (with entrainment) mean thickness estimated from  $\bar{h}(t) \equiv (\bar{\ell}(t) L_y)^{-1} \int_0^{L_y} \int_{x_0}^{X_F(y', t)} h(x', y', t) dx' dy'$ , between a

reference station of  $x_0$  and the leading edge of the density current  $X_F$ . The overflow thickness  $h$  is calculated from  $h(x, y, t) \equiv \int_0^b \delta(x, y, z', t) dz'$  where  $\delta(x, y, z, t) = \begin{cases} 0, & \text{when } S(x, y, z, t) < \epsilon \\ 1, & \text{when } S(x, y, z, t) \geq \epsilon \end{cases}$ . The salinity interface threshold value is taken as  $\epsilon = 0.2$  (psu), since it is the lowest salinity value remaining as a coherent part of the gravity current (fluid particles with lower salinity tend to detach from the current and be advected with the overlying counter flow). Finally,  $\bar{h}_0(t)$  is the original (without any

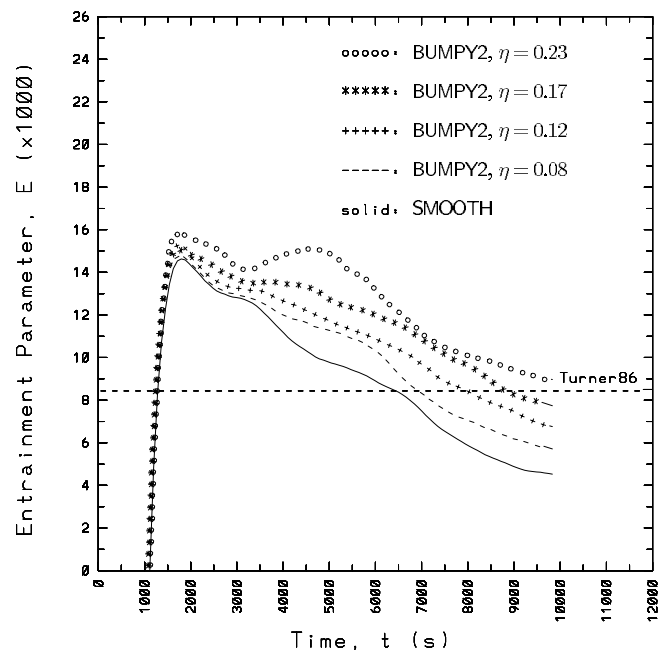


**Figure 3.** Time evolution of entrainment parameters  $E(t)$  in SMOOTH and BUMPY2 for different topographic amplitude factors  $\eta$ . Dashed line marks the estimate  $E = 8.5 \times 10^{-3}$  by Turner [1986].

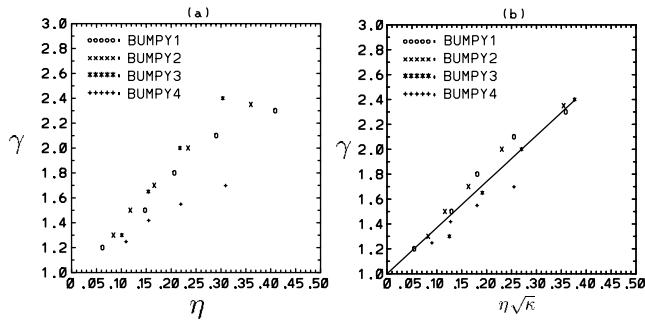


**Figure 4.** The ratio of entrainment in BUMPY and SMOOTH at the end of the simulations,  $\gamma(t = 9830 \text{ s})$  in all experiments, plotted as a function of (a)  $\eta$ , and (b)  $\eta \sqrt{\kappa}$ . The solid line in (b) depicts a least-square fit to data points,  $\gamma \approx 1 + 3.7 \eta \sqrt{\kappa}$ .

entrainment) mean thickness estimated from  $\bar{h}_0(t) \equiv (\bar{\ell}(t) L_y)^{-1} \int_0^t \int_0^{L_y} \int_{z^b+h}^{z^h} u(x_0, y', z', t') dz' dy' dt'$ .

[11] The time evolution of the entrainment parameter  $E(t)$  in SMOOTH is shown in Figure 3. The entrainment parameter decreases with time, because initially entrainment is associated with the growth of the head, which is known to be higher than that in the trailing flow. As the gravity current flows down the slope, the contribution of the head entrainment to overall entrainment decreases. By the time the gravity current reaches the end of the domain,  $E$  appears to reach a steady level of  $E \approx 4.5 \times 10^{-3}$  (but is possibly still decreasing), which is within the approximate range of the estimate  $E = (5 + \theta) \times 10^{-3} = 8.5 \times 10^{-3}$  given by Turner [1986] based on laboratory experiments.  $E(t)$  is calculated for all experiments, and several samples are depicted in Figure 3 for the case of BUMPY2 with different topographic amplitude factors  $\eta$ . As  $\eta$  increases,  $E(t)$  in BUMPY2 exceeds that in SMOOTH. Even for small topographic perturbations ( $\eta = 0.08$ ), there is a notable increase in the entrainment ( $\approx 30\%$ ), and for larger amplitude bumps, the change in the entrainment parameter becomes significant (e.g.,  $\approx 100\%$  for  $\eta = 0.23$ ). Similar results are obtained for all BUMPY experiments.

### 3.3. Parameterization of the Impact of Bumps on Entrainment

[12] In order to quantify the impact of bumpy topography on the entrainment parameter, the ratio  $\gamma(t) \equiv E_{\text{BUMPY}}(t)/E_{\text{SMOOTH}}(t)$  is defined, and calculated at the end of the simulations (at  $t = 9830 \text{ s}$ , approaching a steady state) in all experiments. Figure 4a depicts  $\gamma(t = 9830 \text{ s})$  as a function of  $\eta$  for all experiments, and shows a narrow envelope of data points with a nearly linear relationship. Closer inspection reveals that a certain degree of dependence on the shape of topography persists; while the data envelope is narrow for small  $\eta$  (indicating that the gravity current doesn't feel the difference between different types of bumps for small amplitudes), for larger  $\eta$ , the cases with bottom topographies consisting of high wavenumbers (BUMPY2 and BUMPY3) seem to entrain systematically more than those with lower wavenumbers (BUMPY1 and BUMPY4). This dependence on wavenumbers can be used to further tighten

the scatter of data points by rescaling the  $x$ -axis to include  $\kappa$ , and a simple data regression yields (Figure 4b)

$$\gamma \approx 1 + 3.7 \eta \sqrt{\kappa} \pm 0.1, \quad (1)$$

as a parameterization of the impact of topographic bumps on entrainment in the present set of numerical experiments. Equation (1) quantifies how the entrainment relates to the two parameters of the simulation matrix, the amplitude  $\eta$  and shape  $\kappa$  of the bumps with respect to the underlying slope, which, in principle, can be estimated from high-resolution bathymetric data sets, such as the  $1/30^\circ$  ocean topography database by Smith and Sandwell [1997], or those collected during dedicated observational programs in particular overflow regions.

[13] **Acknowledgment.** The authors acknowledge the support of NSF via grants DMS 0209326 and OCE 0336799, the ONR grant N00014-03-1-0425 and DOE contract W-31-109-ENG-38.

### References

- Baines, P. G. (2001), Mixing in flows down gentle slopes into stratified environments, *J. Fluid Mech.*, **443**, 237–270.
- Beckmann, A., and R. Döschner (1997), A method for improved representation of dense water spreading over topography in geopotential-coordinate models, *J. Phys. Oceanogr.*, **27**, 581–591.
- Fischer, P. F. (1997), An overlapping Schwarz method for spectral element solution of the incompressible Navier-Stokes equations, *J. Comput. Phys.*, **133**, 84–101.
- Fischer, P. F., and J. S. Mullen (2001), Filter-based stabilization of spectral element methods, *C. R. Acad. Sci., Ser. I*, **332**, 265–270.
- Goff, J. A., and T. H. Jordan (1988), Stochastic modeling of seafloor morphology: Inversion of sea beam data for second-order statistics, *J. Geophys. Res.*, **93**, 13,589–13,608.
- Özgökmen, T. M., and E. Chassignet (2002), Dynamics of two-dimensional turbulent bottom gravity currents, *J. Phys. Oceanogr.*, **32**, 1460–1478.
- Özgökmen, T. M., P. Fischer, J. Duan, and T. Iliescu (2004), Three-dimensional turbulent bottom density currents from a high-order nonhydrostatic spectral element model, *J. Phys. Oceanogr.*, in press. (Available at <http://www.rsmas.miami.edu/personal/tamay/3D/gc3d.pdf>.)
- Özsoy, E., D. D. Iorio, M. C. Gregg, and J. O. Backhaus (2001), Mixing in the Bosphorus Strait and the Black Sea continental shelf: Observations and a model of the dense outflow, *J. Mar. Syst.*, **31**, 99–135.
- Papadakis, M. P., E. P. Chassignet, and R. W. Hallberg (2003), Numerical simulations of the Mediterranean Sea outflow: Impact of the entrainment parameterization in an isopycnic coordinate ocean model, *Ocean Modell.*, **5**, 325–356.
- Price, J. F., and M. O. Baringer (1994), Outflows and deep water production by marginal seas, *Prog. Oceanogr.*, **33**, 161–200.
- Price, J. F., M. O. Baringer, R. G. Lueck, G. C. Johnson, I. Ambar, G. Parrilla, A. Cantos, M. A. Kennelly, and T. B. Sanford (1993), Mediterranean outflow mixing and dynamics, *Science*, **259**, 1277–1282.
- Smith, W. H. F., and D. T. Sandwell (1997), Global sea floor topography from satellite altimetry and ship depth soundings, *Science*, **277**, 1956–1962.
- Turner, J. S. (1986), Turbulent entrainment: The development of the entrainment assumption, and its applications to geophysical flows, *J. Fluid Mech.*, **173**, 431–471.
- Weissel, J. K., L. F. Pratson, and A. Malinverno (1994), The length-scaling properties of topography, *J. Geophys. Res.*, **99**, 13,997–14,012.
- Willebrand, J., B. Barnier, C. Böning, C. Dieterich, P. Harraann, P. D. Killworth, C. LeProvost, Y. Jia, J.-M. Molines, and A. L. New (2001), Circulation characteristics in three eddy-permitting models of the North Atlantic, *Prog. Oceanogr.*, **48**, 123–161.

T. M. Özgökmen, RSMAS/MPO, University of Miami, Miami, FL 33149-1098, USA. (tozokmen@rsmas.miami.edu)

P. F. Fischer, Mathematics and Computer Science Division, Argonne National Laboratory, Argonne, IL 60439, USA.

J. Duan, Department of Applied Mathematics, Illinois Institute of Technology, Chicago, IL 60616, USA.

T. Iliescu, Department of Mathematics, Virginia Polytechnic Institute and State University, Blacksburg, VA 24061, USA.